Astron. Astrophys. 221, 311–320 (1989)

ASTRONOMY AND ASTROPHYSICS

Is HS 240 an interstellar bubble?*

L. Wisotzki ** **and H. J. Wendker**

Hamburger Sternwarte, Gojenbergsweg 112, D-2050 Hamburg 80, Federal Republic of Germany

Received January 2, accepted March 9, 1989

Summary. We present radio, optical, and infrared observations of the galactic H II region HS 240 = S 119 around the O 7,5V star 68 Cyg. No evidence is found that the extended nebular structure may have formed under the action of a strong stellar wind. The measured emission line strengths are typical for a low-excitation nebula. The electron temperature, derived from optical line widths, is (7500 ± 1000) K. The large scale emission measure distribution is rather uniform, with an average electron density of $\sim 2\,\mathrm{cm}^{-3}$. There are indications that at least part of the gas is concentrated in small clumps of densities not higher than $\sim 100\,\mathrm{cm}^{-3}$. The measured dust colour temperature is 41 K averaged over the whole H II region. The infrared emission distribution – not ring-like but centered on the star – demonstrates that the inner region is not a wind-blown cavity. We show that due to the high peculiar velocity of 68 Cyg the wind front may not reach further than ~ 1 pc from the star, i.e. less than 5% of the radius of the H II region, and a bow shock instead of a bubble is created. We present high-resolution IRAS data where this bow shock is indeed visible.

Key words: interstellar bubbles – bow shocks – H II regions – infrared radiation – radio radiation – emission lines – HS 240 – 68 Cyg

1. Introduction

Strong stellar winds from early-type stars may blow huge cavities or "bubbles" into the interstellar medium. While the physics of these processes has been extensively discussed (standard paper of Weaver et al., 1977; hereafter quoted as WEA), the observational data base is still somewhat short. A number of ring nebulae around WR stars have been classified as wind-driven bubbles (Chu, 1981), but the number of bubbles around "normal" O- and Of stars is much smaller than the abundance of O stars in the galactic plane would suggest. Lozinskaya's (1982) list features only two entries of this type: NGC 7635 (the well-known "bubble nebula"), and HS 240.

The extended, faint H II region HS 240 = S 119 (Hase and Shajn, 1955; Sharpless, 1959) covers an area of $\sim 3^\circ \times 3^\circ$ around the O 7.5 star 68 Cyg (HD 203064, BD +43 3877, $\alpha(1950.0) = 21^\mathrm{h}16^\mathrm{m}35^\mathrm{s}.2$, $\delta(1950.0) = +43^\circ 44' 06''$). It had not been of any particular interest until Lozinskaya (1982) proposed – on grounds of its optical appearance – that its ring-like structure had formed under the action of a strong wind from 68 Cyg.

The amount of observational data collected up to now is not conclusive. The best radio map was supplied by Wendker (1971) at 1400 MHz, with low sensitivity. Felli et al. (1977) and Esipov et al. (1982) published fan-beam scans with poor resolution at 408 and 102 MHz, respectively. Pedlar (1980) observed the brightest part in the H 166α line and reported a radial velocity of $+1.4\,\mathrm{km\,s}^{-1}$ and an LTE electron temperature of 4750 K. Optical interferometry was done by Georgelin and Georgelin (1970) and in greater detail by Esipov et al. (1982). According to them the nebula shows chaotic motions rather than ordered expansion (upper limit $v_\mathrm{exp} \leqq 15\,\mathrm{km\,s}^{-1}$), and the mean LSR radial velocity is $+(6 \pm 1)\,\mathrm{km\,s}^{-1}$. Esipov et al. (1982) also determined relative intensities of emission lines at five spectrograph slit positions. However, their conclusion that all observations support the bubble model for HS 240 is not convincing.

Distance determinations of the exciting star 68 Cyg (O 7.5 V; Zeĭnalov et al., 1987), range from 720 pc (Bouigne, 1959) to 880 pc (Alduseva et al., 1982), corresponding to a bolometric luminosity of $0.8 \ldots 1.2\ 10^5\ L_\odot$. Its radial velocity varies around $-10\,\mathrm{km\,s}^{-1}$ (Alduseva et al., 1982; Hänni and Pelt, 1986; Zeĭnalov et al., 1987). It is an X-ray source (Kumar et al., 1983), and a runaway star with a peculiar velocity of $41.6\,\mathrm{km\,s}^{-1}$, leaving the Cyg OB7 association almost exactly in $-b^{II}$-direction (Stone, 1979). A crude age estimate of $\sim 2.5\ 10^6$ yr may be obtained by applying De Loore's (1978) evolutionary tracks, not too far away from Stone's (1979) kinematic age of $1.5\ 10^6$ yr. The mass loss rate has not yet been determined; it can be estimated to $\dot{M} \simeq 1 \ldots 5\ 10^{-7}\ M_\odot\,\mathrm{yr}^{-1}$ using the formulae given by Chiosi and Maeder (1986 and references therein). The terminal wind velocity was measured by Black et al. (1980) to $v_\infty = 2900\,\mathrm{km\,s}^{-1}$; recently Prinja and Howarth (1988) obtained 2520–2740 $\mathrm{km\,s}^{-1}$ from high resolution spectra of the Si VI $\lambda\lambda$ 1394, 1403 doublet. The appropriate equation given by Panagia and Felli (1975) leads to an expected radio flux density for such a wind of less than 0.1 mJy at 5 GHz. This is far below published upper limits (e.g. Wendker, 1987) or the one derived in Sect. 2.1.

Send offprint requests to: H. J. Wendker

* Radio observations were carried out at the 100 m radio telescope Effelsberg, operated by the Max-Planck-Institut für Radioastronomie Bonn. The IRAS data have been processed using the GEISHA analysis system developed by the Laboratory for Space Research and University of Groningen, Groningen, The Netherlands

** Visiting Astronomer, German-Spanish Astronomical Center, Calar Alto, operated by the Max-Planck-Institut für Astronomie, Heidelberg, jointly with the Spanish National Commission for Astronomy

We have performed a detailed multifrequency study of the nebula and present in Sect. 2 data from radio continuum and line observations, optical spectroscopy, and far infrared mapping. The interpretation and determination of overall physical properties in Sect. 3 was possible by using simple static models. In Sect. 4 we discuss the influence of the stellar wind, some observational implications, and try to sketch a consistent picture of the nebular history, including the effects of the rapid stellar motion. In Sect. 5 we present our conclusions. Finally, a short appendix gives some formulae used in the model calculations.

2. Observations

2.1. Radio continuum mapping

The observations were carried out in August 1987 with the 100 m telescope in Effelsberg, recording total power with a filter bandwidth of 20 MHz centered at 1410 MHz. Both polarization channels were calibrated separately using the sources 3C 48, 3C 147, 3C 286, 3C 348 (flux densities at 1400 MHz according to Baars et al., 1980) and averaged.

The HPBW was 9.′2 circular. An area of $4° \times 4°$ was covered at least twice by the mapping procedure, giving a grid size of $20^s = 3.'5 \times 1.'02$. The data reduction was done interactively and featured the usual steps: radar spike elimination, averaging, baseline correction, smoothing and reduction of the oversampling to a final grid of $20^s \times 3'$. The mean uncertainty in the inner parts of the map is ± 100 mK brightness temperature, and is mainly determined by the uncertainties in fixing a realistic underlying zero level. To minimize the scan-to-scan variations the composite map was slightly smoothed in right ascension direction with a Gaussian of three scans HPBW.

The resulting map, given in Fig. 1, shows that the projected H II distribution is rather uniform with deviations not higher than a factor of 2–3 over a large elliptical area, where the exciting star 68 Cyp is remarkable off-centre. An integration of the nebular emission within the 200 mK contour yields a total flux densities of (43.4 ± 1.4) Jy, where the contributions of the marked point sources (Table 1) are already substracted. These are definitely non-thermal background sources.

We also mapped HS 240 at 4.8 GHz in Effelsberg during May/June 1985, where we unfortunately suffered from initially not recognized bad atmospheric conditions so that a baseline correction could not be established in a satisfying way. The resulting map was not usable for faint structure studies. Only a flux density integration could give an acceptable value, calibrated against NGC 7027 (Wendker, 1984). We obtained $S_{4.8\,\mathrm{GHz}} = (40 \pm 5)$ Jy. The spectrum of HS 240 can in this way be clearly identified as originating solely from optically thin, thermal radiation, with a spectral index of $\alpha = -0.07 \pm 0.1$ ($S_\nu \propto \nu^\alpha$).

The map allows to deduce an upper limit of 7 mJy (3σ) for the flux density of a point source at the position of 68 Cyg. This is much fainter than hitherto published values and corresponds to an upper limit for $\dot{M}$ of $5\ 10^{-5}\ M_\odot\ \mathrm{yr}^{-1}$.

2.2. Observations in the 21 cm line

During the Effelsberg session in August 1987 we also obtained a set of H I spectra at 1420 MHz with 0.64 km s^{-1} spectral resolution and an rms noise of ~ 1 K T_b. Since the available observation time did not allow to perform a complete coverage, a field between 42° and 45° and 21^h08^m and 21^h28^m was crossed by ten raster scans, resulting in a grid of spectra with spacings $40^s = 7.'2 \times 15'$.

The data were displayed in form of grey scale maps for different radial velocities; our main intention was to check whether a neutral H I shell around the H II region or at least an H I depletion in the direction of 68 Cyg is visible. In Fig. 2 four sample maps are shown.

At radial velocities less than ~ 5 km s^{-1} no trace of a shell or arc-like structure is visible. At higher positive velocities the expanding giant shell GS 088-04+17 detected by Heiles (1979) becomes the dominating feature. Around its central RV of ~ 17 km s^{-1} it has a diameter of $\sim 5°$ and is larger than the mapped frames. A possible physical association with HS 240 is excluded.

2.3. Spectroscopy of optical emission lines

The observations were performed with the 2.2 m telescope at Calar Alto in June 1987, using the coudé spectrograph, the f/3 camera

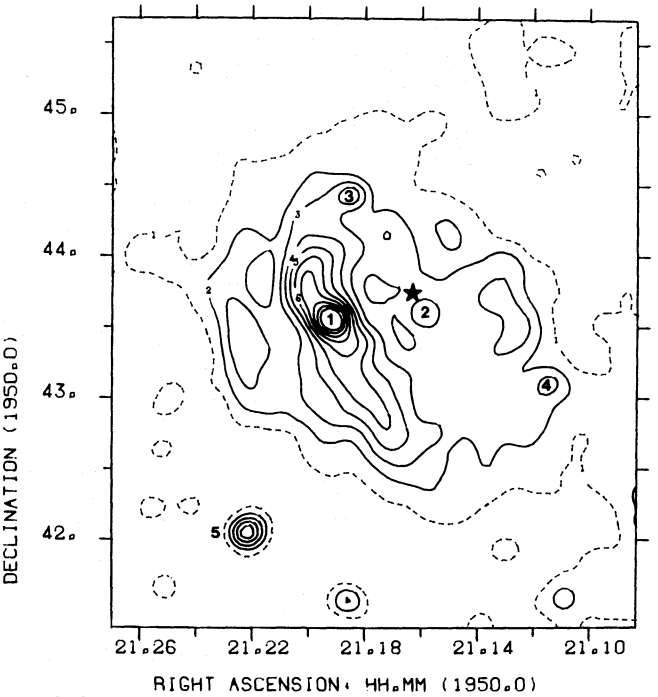

Fig. 1. Radio continuum map of HS 240 at 1410 MHz. Contour units are 200 mK brightness temperature. Here and in the following figures the position of 68 Cyg is denoted by an asterisk

Table 1. Marked point sources in the 1410 MHz map. The 408 MHz fluxes are from unpublished DRAO-SRT observations by Caswell et al.

Nr.	Identification	S_{1410}	S_{408}
1	4C 43.52	0.70 Jy	2.08 Jy
2	B3 2116+436	0.18	0.40
3	B3 2118+444	0.28	0.44
4	B3 2111+432	0.18	0.79
5	VRO 42.21.01	0.55	1.38

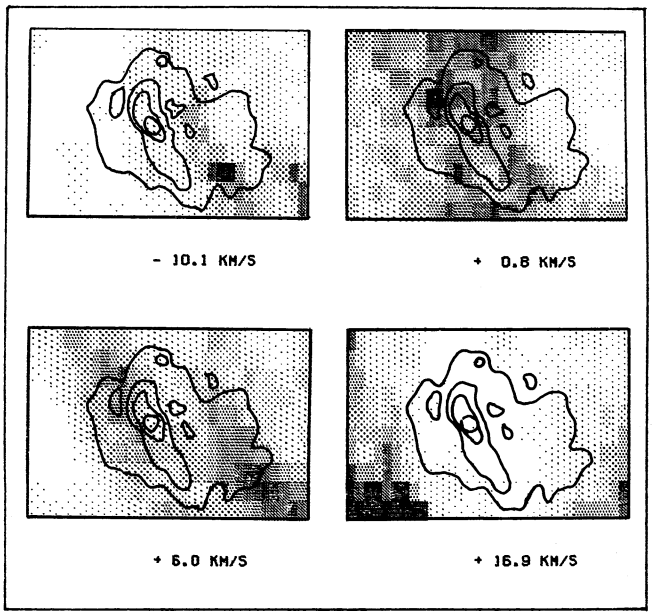

Fig. 2. Channel maps at −10.1, +0.8, +6.0, and +16.9 km s^{-1}. Superimposed are contours of the continuum map. Grey scales are adjusted individually to the dynamic range of each map (brightness temperature), with black as maximum

with 8.5 Å mm^{-1} dispersion in 2nd grating order, and a CCD detector of type RCA. The slit length was 117″, the spectral pixel resolution at Hα 11.7 km s^{-1}. At nine slit positions, selected from the optical appearance, spectra of H, [N II], [S II], and [O III] lines were taken. In Fig. 3 these positions are superimposed on a red colour photograph taken with the 80 cm Schmidt telescope at Calar Alto.

Due to the low surface brightness of HS 240 even in the brightest parts the weak lines [N II] λ5755 and [O III] λ4363 could not be detected. The line pair [O II] λλ3726, 3729 was not observable due to technical reasons.

The reduction of the two-dimensional CCD frames followed standard procedures. After wavelength calibration and rebinning all spectra were converted to one-dimensional data sets by integrating over the whole slit length. This was justified because no spectra displayed any significant variations over the slit coordinate. The S/N ratio could thus be increased up to ~20–50 in Hα. In order to eliminate the spectral response of the detector the observed spectra of 68 Cyg were compared with Kurucz' (1979) model calculations for a star of $T_{\rm eff} = 35000$ K and $\log g = 4$.

For each spectral line its line integral and the two highest pixel values were measured. allowing the determination of the line halfwidth with a correction for a line center offset from the corresonding pixel center. To fit a Gaussian to such narrow profiles was rejected because of the large influence of noise in the line wings.

The width of Hα may be significantly increased by fine structure line splitting (Dyson and Meaburn, 1971). The corresponding values were corrected for this effect; in Tables 2 and 3 all measured line intensities and halfwidths are listed. The values in square brackets had a low S/N ratio and were not used in the further evaluation.

2.4. *Far-infrared mapping*

From the IRAS all sky survey low resolution maps at wavelengths 100 and 60 μm were extracted, using the SPLINE datasets prepared at the Laboratory for Space Research, Groningen. The maps in equatorial coordinates have pixel spacings $12^s \times 3'$ and a resolution of $32^s \times 8'$. To convert the given in-band fluxes into flux densities a blackbody spectrum of $T = 30$ K was assumed. The global background was removed by fitting a bilinear "twisted plane" to the outer regions of the map.

In both maps (Figs. 4 and 5) the H II region is clearly visible. The emission in the 60 μm map is dominated by the inner parts of the region, with a prominent concentration around 68 Cyg. The diagonal rifts in the north-western corner are spurious.

The total flux densities were obtained by integrating inside the 5 MJy sr^{-1} contour of the 60 μm map; the results are $S_\nu(100\,\mu m) = 2.2\ 10^4$ Jy and $S_\nu(60\,\mu m) = 9.6\ 10^3$ Jy. A blackbody of $T = 41$ K would have the same flux ratio.

2.5. *High resolution infrared imaging*

A search for infrared structures on the arcmin scale in the central region was performed by applying the high resolution software of the GEISHA system (Wesselius et al., 1987) to a field measuring $0.^\circ5 \times 0.^\circ5$ around 68 Cyg. The image reconstruction involves an iterative procedure which couples gain in resolution with strong noise increase. Since in the 60 μm wavelength band the warm dust close to 68 Cyg should show up most prominently, we chose this as the prime band for the analysis.

The reconstructed image is displayed as a contour line plot in Fig. 6. The spatial resolution is better than 2′ and thus close to the diffraction limit of the IRAS aperture (~1′). The positional offset of 68 Cyg to the brightest parts of the region is remarkable. The small-scale structure forms a slightly curved ridge in the south east of the star. The source marked by an arrow may be identified with an entry in the IRAS point source catalog and is probably extragalactic. A rough flux calibration was obtained by comparing the integrated flux of the inner $15' \times 15'$ with the corresponding number of the SPLINE map. However, the total flux is not conserved by the resolution-enhancement algorithm.

2.6. *Intercomparison*

The large scale morphology of HS 240 can be characterized by three distinct components:

1. A diffuse, featureless background present in all three wavelength regimes, extending over a size of ~2°.

2. Bright elongated filaments, prominent especially in the (extinction-contaminated) optical image where some kind of a ring structure may be seen. While in the radio map these features are much less dominating compared to the background than in the uncalibrated photograph, only rudiments can be traced in the infrared.

3. The central zone around 68 Cyg. It is the most prominent part in the SPLINE and spatially resolved in the GEISHA image; it has an emission minimum in the optical (but note again the extinction lanes), and it displays nothing particular in the radio map (though a structure on the arcminute scale would be completely smoothed out by the telescope beam).

In the following sections we will evaluate these data, and the physical conditions they reflect.

3. Interpretation

3.1. *Electron temperature*

Since the temperature sensitive auroral lines turned out to be not detectable, a kinetic temperature was derived from the widths of

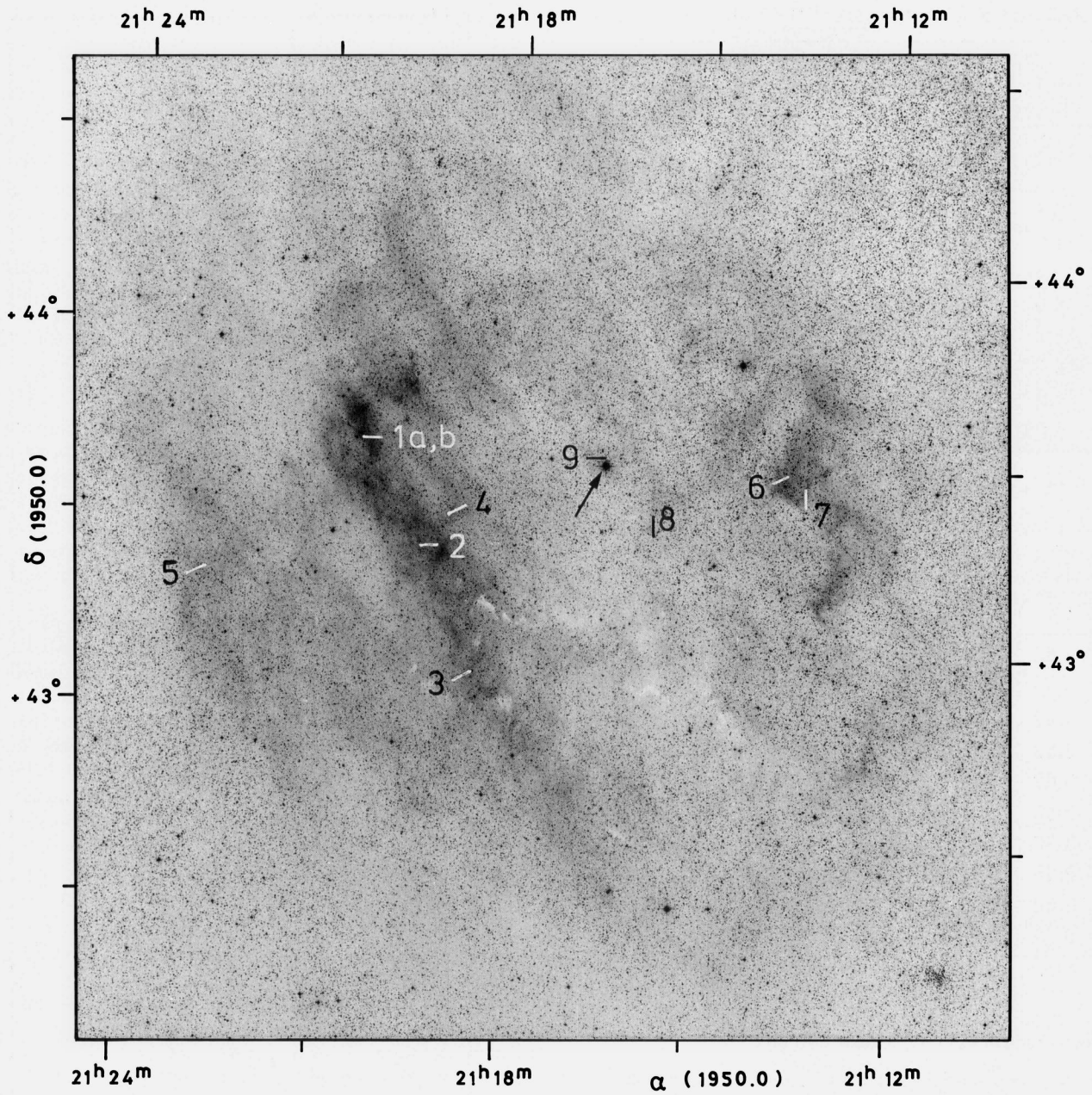

Fig. 3. Slit positions of optical spectra. Positions 1a and 1b are only slightly shifted. 68 Cyg is here marked by an arrow

the observed emission lines. The necessary assumption that no macroturbulences broaden the lines with a non-Gaussian function was strongly supported by the structure of the two-dimensional long slit spectra. Microturbulences and apparatus profile should be equal for all lines, whereas thermal Doppler broadening mainly should affect the Hα widths. The most critical assumption is that of equal column density ratios of the H^+, N^+, and S^+ species.

Using $s^2_{\text{Doppler}} = s^2_{\text{obs}} - (s^2_{\text{turb}} + s^2_{\text{app}})$, the kinetic temperature is

$$T_e = 4.91\ 10^4\ \{s^2(\text{H}\alpha) - s^2[\text{N II}]\}\ \text{K}$$

$$T_e = 4.59\ 10^4\ \{s^2(\text{H}\alpha) - s^2[\text{S II}]\}\ \text{K}$$

with the measured widths s given in Å. We have evaluated all entries of Table 3 except those marked by square brackets. Although the individual scatter is not low, the data show a prominent concentration between 7000 and 8000 K. As a final temperature we adopt the value

$$T_e = (7500 \pm 1000)\ \text{K},$$

where the error is our conservative estimate.

Although this is somewhat higher than the 4750 K of Pedlar (1980), we find it still in agreement with the ionization status of HS 240 (cf. below), considering that both methods not necessarily weight all volumes equally. The temperature of 12000 K given by Lozinskaya (1982), on the other hand, is not supported by observational evidence.

Table 2. Relative line fluxes in terms of Hα = 100

Slit	[N II]		[S II]		[O III]
	λ6548	λ6583	λ6716	λ6731	λ5007
1a	11.7	36.5	17.2	11.6	2.7
1b	—	—	16.0	12.4	—
2	10.1	36.0	23.2	17.4	3.9
3	11.0	39.6	17.9	12.1	—
4	10.4	34.8	—	—	—
5	15.9	58.5	28.6	23.5	—
6	10.9	36.3	17.0	11.7	—
7	16.2	48.9	25.6	17.4	—
8	9.0	29.9	—	—	—
9	9.0	20.8	—	—	—

Table 3. Line widths (FWHM) in Å

Slit	H_α	[N II]		[S II]	
		λ6548	λ6583	λ6716	λ6731
1a	0.66	0.44	0.44	0.43	0.40
1b	—	—	—	0.39	0.43
2	0.62	0.37	0.42	0.39	0.41
3	0.58	0.40	0.47	0.41	0.41
4	0.62	0.46	0.47	—	—
5	0.60	0.44	0.43	0.43	0.47
6	0.58	0.48	0.43	0.45	0.41
7	0.65	0.49	0.46	0.47	0.45
8	0.68	[0.69]	0.57	—	—
9	0.73	[0.39]	0.55	—	—

3.2. *Density distribution*

The observed radio brightness distribution of the nebula is determined by the emission measure $\varepsilon \equiv \int n_e n_p \, dz \simeq \int n_0^2 \, dz$, with n_0 as general hydrogen density. Using the expression of Mezger and Henderson (1967) for the optical depth and assuming $T_e = 7500$ K, the brightness temperatures T_b (in K) can be converted directly into emission measure:

$$\varepsilon = 568 \, T_b \, \mathrm{cm}^{-6} \, \mathrm{pc} .$$

For a homogeneous Strömgren sphere with known excitation parameter u the emission measure in central line of sight ε_s is directly related to the mean density n_0 and the Strömgren radius R_s. A mean ε_s of 250 cm^{-6} pc was estimated near 68 Cyg; with u between 37 and 50 $\mathrm{pc\,cm}^{-2}$ (see discussion below) the derived parameters are

$$n_0 = 2.0 \ldots 2.5 \, \mathrm{cm}^{-3}, \quad R_s = 20 \ldots 32 \, \mathrm{pc} .$$

Another estimate can be obtained by evaluating the total flux density and assuming spherical symmetry (Mezger and Henderson, 1967). However, the uncertainties in the adopted distance d

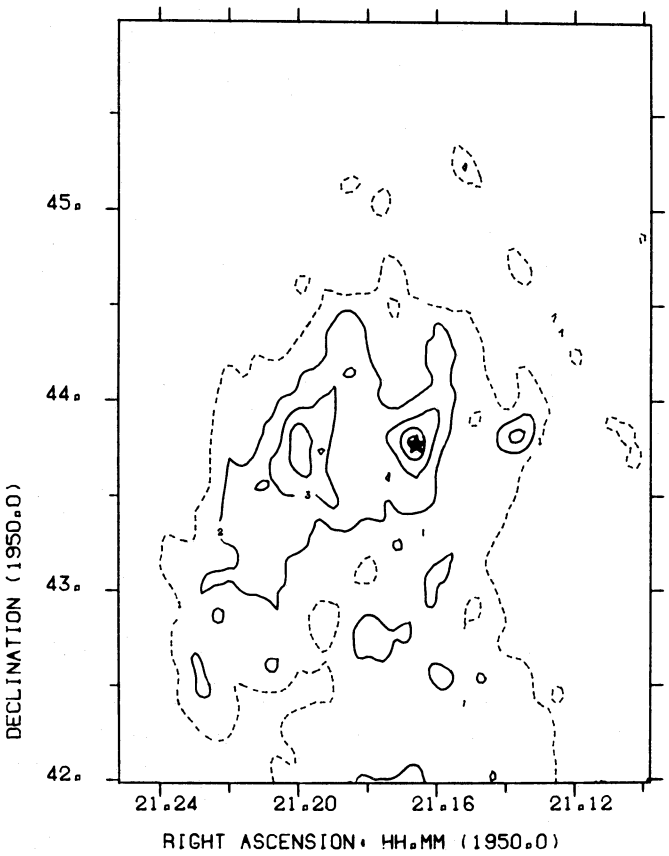

Fig. 4. IRAS map of HS 240 at 100 μm. Contour units are 10 MJy sr^{-1}

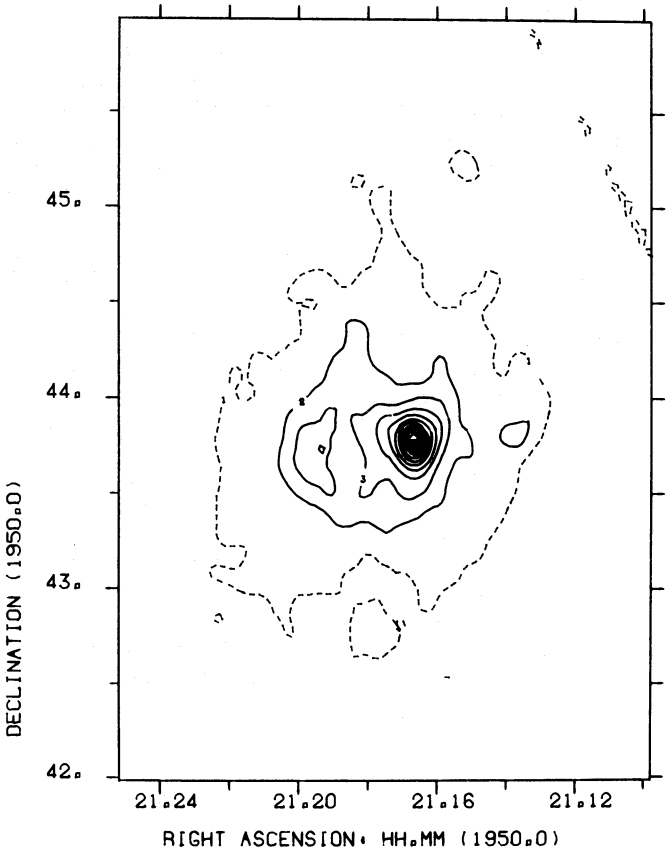

Fig. 5. IRAS map of HS 240 at 60 μm. Contour units are 5 MJy sr^{-1}

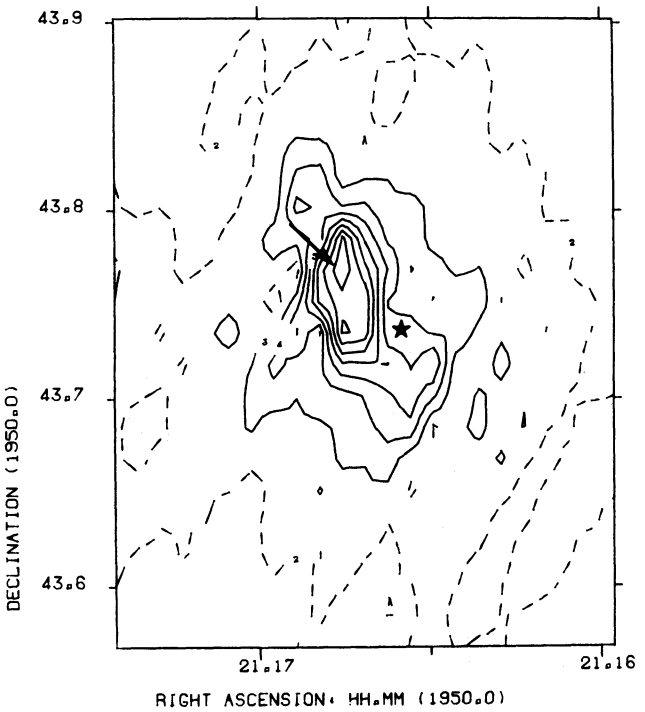

Fig. 6. Inner part of the high resolution IRAS map around 68 Cyg at 60 μm. The point source marked by an arrow is probably extragalactic. Contour units are 20 MJy sr^{-1}

and angular diameter ϑ_s yield large errors in the result. With $d = (800 \pm 80)$ pc and $\vartheta_s = (150 \pm 30)'$ one gets

$n_0 = (1.7 \pm 0.8)\,\mathrm{cm}^{-3}$.

The assumption of a homogeneous density obviously is a strong oversimplification. To model the observed brightness fluctuations both density and H^+ path length may be adjusted, depending on the assumed geometry. In the centre of the bright western rift the emission measure is about 500 cm^{-6} pc (without the extragalactic point source). A "cigar shaped" cloud with diameter 3 pc would have $n \simeq 10\,\mathrm{cm}^{-3}$, a shell geometry would require $n \simeq 6\,\mathrm{cm}^{-3}$, and a fit to the column depth of the whole H II region would alter the mean density along the line of sight to only $n \simeq 3\,\mathrm{cm}^{-3}$.

The measurement of local space densities via the [S II] $I(\lambda 6716)/I(\lambda 6731)$ line ratio is independent of geometrical considerations. Using the calibration diagram published by Aller (1984), densities at seven positions could be obtained which are summarized in Table 4.

In three cases the values are significantly higher than the mean density. Note that the other values derived are close to the low density limit of the line ratio. It must be stressed that the brightest filaments are not necessarily identical with the densest clumps: The maximum value of $n_e = 130\,\mathrm{cm}^{-3}$ is found in the relatively faint zone around position 5.

To summarize, we state that the large-scale density distribution is very uniform, with small embedded clumps of higher density which apparently have not yet evaporated by thermal pressure or stellar radiation.

3.3. *Stellar radiation field and ionization balance*

The excitation parameter of the ionizing star (or the number of Lyman continuum photons N_{Lc}) can be derived from the total flux

Table 4. Local densities in HS 240

Slit position	n_e/cm^{-3}
1a	10 – 20
1b	90
2	60
3	10 – 20
5	130
6	10 – 20
7	10 – 20

density, if the H II region is optically thick in the Lyman continuum. Application of the formula given by Schraml and Mezger (1969) yields

$u = 42.1 \ldots 36.8\,\mathrm{pc\,cm}^{-2}$

depending upon the assumed distance. This is much less than expected for a star of type O7.5 V (50 pc cm^{-2}; Georgelin et al., 1975), a factor 2 or more wrong in N_{Lc}. Such a discrepancy is a typical indication that the H II region is at least partially density-bound. The deviation of line-of-sight extension from the projected radius especially in the north-western direction supports this interpretation. On the other hand the calibration spectral type vs. u is known to be not very accurate; it may well be that part of the problem is caused by a too high theoretical value for u.

To obtain the approximate ionization status of the H II region the measured line intensities of Hα, [N II], [S II], and [O III] were evaluated. Assuming cosmic abundances and a stellar radiation field characterized by $T_{\mathrm{eff}} = 33000$ K, the figures fit well into the sequence of static photoionization models calculated by Stasinska (1978). The prominent [N II] and [S II] features as well as the extremely faint [O III] lines are typical for a low-excitation nebula with O^+ as major cooling species. Since cooling is less effective than in H II regions with much [O III], the equilibrium electron temperatures are somewhat higher and may well reach 7000 K. The agreement of observations with model calculations is even better for a non-homogeneous ISM where the gas is concentrated in small dense clumps.

There is no indication of collisional ionization and excitation as observed in strong radiative shocks.

3.4. *Large-scale dust distribution*

The physical properties of interstellar dust grains are still not well exploited. In our discussion of the infrared maps we therefore limit ourselves to rough approximations and qualitative considerations, aiming mainly at a consistency check between theory and observations.

The far-infrared emission of radiatively heated dust grains in H II regions originates almost solely from a degradation of stellar UV quanta. Since the low-density nebula HS 240 is optically thin to all stellar radiation longwards of the Ly-limit (unlike *compact* H II regions), the dominating heating source is the diffuse Lα photon field which is in turn produced by the H ionization-recombination process (Spitzer, 1978). Virtually every Lyman continuum photon yields a Lα quantum, so that the total diffuse Lα luminosity is directly proportional to the number of Lc photons the star emits. For 68 Cyg a value of $L(\mathrm{L}\alpha) = 8.2\ 10^{37}\,\mathrm{erg\,s}^{-1}$ was thus obtained. The dust heating

function depends, however, only on the local H^+ density and the grain size. The cooling by IR emission, on the other hand, involves the emission efficiency which is difficult to determine. With its Planck-average taken from Draine and Lee (1984), we may write the condition of thermal balance as

$$1.71\ 10^7 n_e = a \cdot T_d^6$$

with n_e: electron density in cm^{-3}, a: grain radius in μm, and T_d: dust temperature in K.

Most of the dust mass is represented by grains of the dimension $a \simeq 0.1$ μm. With the mean density in HS 240 of $n_0 = 2\,cm^{-3}$, the steady-state dust temperature would be ~ 26 K, a value much below the observed colour temperature of 41 K. This discrepancy can be solved if one considers that much of the gas is concentrated in small clumpings of density $\sim 10 \ldots 100\,cm^{-3}$. The dust distribution must similarly be non-uniform (the gas-dust coupling in H II regions is very strong because of the large grain surface charge; Spitzer, 1978). The corresponding dust temperatures would rise to 34 ... 50 K.

To model the total flux density of HS 240 at 60 μm, the calculated Lα luminosity was simply equated with the total IR radiation power. Assuming a blackbody spectrum with $T_{eff} = T_c = 41$ K, the corresponding flux density at 60 μm is $1.2\ 10^4$ Jy, in excellent agreement with the observed value of $0.96\ 10^4$ Jy.

The expected surface brightness was calculated using a Planck emissivity B_ν; the optical depth through the nebula is given by (Spitzer, 1978)

$$\tau = 1 - 10^{-0.4 A_v} = 1 - 10^{-2.64\ 10^{-3} n_H z}$$

where z is the column depth given in pc. The flux density at 60 μm per solid angle is then for $n_H = 2\,cm^{-3}$ and $z = 10$ pc

$$S_\nu = 1.9\ 10^7\,Jy\,sr^{-1}$$

which again agrees well with the observations (cf. Fig. 5).

The morphology of the HS 240 dust complex in the 60 μm SPLINE map exhibits three distinct zones: a) a very bright concentration around 68 Cyg with a diameter of only ~ 5 pc; b) a fairly uniform elliptical area of 15×20 pc; and almost no emission from c) the outermost parts. This tendency is easy to understand as a consequence of the different heating conditions: In the large zone b) Lα heating is dominating, whereas towards the edge of the H II region the ionized fraction of H decreases and Lα quanta may escape from the H II region, thus reducing the energy density of the diffuse radiation field. On the other hand, in a distance of $r \simeq 3.5$ pc the direct stellar radiation becomes comparable to the diffuse photon field; hence, close to the star both the dust temperature and the IR flux will increase. However, within the static scenario employed up to now, the structure of the central region as visible in the high resolution GEISHA map cannot be explained. The dust emission should rise symmetrically towards the central star and peak at its very location. We discuss this phenomenon at the end of the next section.

4. Stellar wind and ISM

The introduction of the wind-driven bubble hypothesis to explain the approximate ring shape of HS 240 leads to observational consequences, some of which we will discuss here. We adopt the terminology of WEA for the four different zones forming the bubble: region **a** is the freely streaming stellar wind, region **b** the hot, shocked wind driving the expansion by thermal pressure, region **c** consists of compressed interstellar gas swept up by an isothermal shock, and region **d** is the ambient interstellar medium, mostly an H II region.

4.1. *The age of the bubble*

Since no systematic expansion of any parts of HS 240 is observable (Esipov et al., 1982), a kinematic age can only be estimated from the present inner radius of the "ring" by applying the expansion formula of Castor et al. (1975) for an "energy-conserving" bubble. With $n_0 = 2\,cm^{-3}$, $\dot{M} = 1 \ldots 5\ 10^{-7} M_\odot\,yr^{-1}$, and $v_\infty = 2900\,km\,s^{-1}$, the bubble age follows to $t_b = 3 \ldots 5\ 10^5$ yr, which is far below the approximate stellar age. Furthermore, the highly asymmetric structure of the "HS 240 ring" makes it difficult to believe that still a hot bubble interior as described by WEA drives forth the outer shell. McKee et al. (1984) have shown that an "energy conserving bubble" cannot survive in a clumpy medium: radiative losses soon exceed the wind luminosity, so that region **b** collapses, and the expansion continues rather following the simpler momentum conserving case. But such a bubble would already stall at a radius of ~ 10 pc and dissipate into the ambient medium; hence, no information about its age were available. Certainly this picture would be in better agreeement with the HS 240 morphology, but it must be stressed that such an old, dissipating bubble looks not very different from any accidentally ring-shaped H II region.

In Appendix A we show that the condition given by WEA under which the ionization front may be trapped in shell **c** must be corrected. As a result we state that generally H I shells around extended O star bubbles should occur quite exceptionally. Hence, the absence of any shell- or arc-like feature in the 21 cm channel maps that can be associated with HS 240 does not set constraints to the physical conditions.

4.2. *Wind-blown dust*

The distribution of the radiatively heated dust provides an independent insight into the structure of a bubble. The strong gas-dust coupling (cf. above) ensures that the dust distribution in an H II region resembles mainly the gas morphology. Van Buren and McCray (1988) recently reported IRAS observations of dust rings around WR stars bubbles.

The IRAS maps of HS 240 show no trace of a ring-like structure in the regions of interest. Contrarily, the 60 μm SPLINE map (Fig. 5) exhibits a strong concentration of dust emission towards the center. As discussed above, this is in full agreement with the heating processes in a "normal" H II region. The infrared emission from the almost depleted interior of a bubble would certainly look different, so that the standard bubble model can be ruled out for HS 240.

4.3. *Motion of the blowing star*

According to Stone (1979), 68 Cyg is a runaway star probably originating close to the center of the Cyg OB7 associaction, moving with a peculiar velocity of $41.6\,km\,s^{-1}$ from north west towards south east through the HS 240 area. The interaction of the ISM with a stellar wind emanating from a star moving supersonically with $v_* \simeq 4 c_{II}$ differs considerably from that in models with the star at rest. A bow shock rather than a closed bubble will form, and a hot interior of shocked stellar wind material will not exist. Furthermore, in backward direction to the stellar motion a cone of

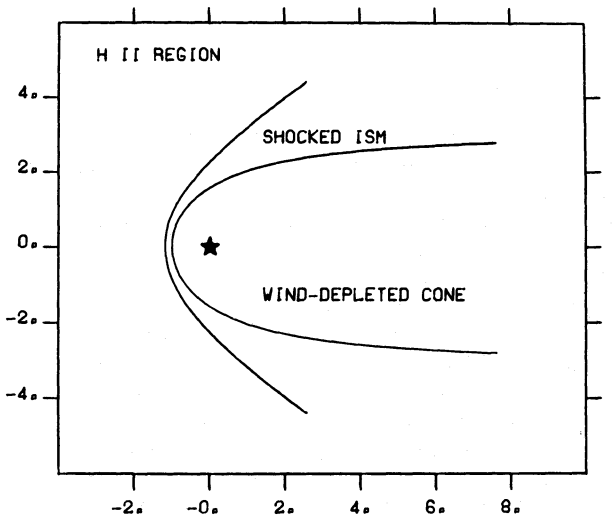

Fig. 7. Modelled bow shock around a rapidly moving star. Length unit scales with the *standoff* distance $R_1(0)$ (cf. Appendix B)

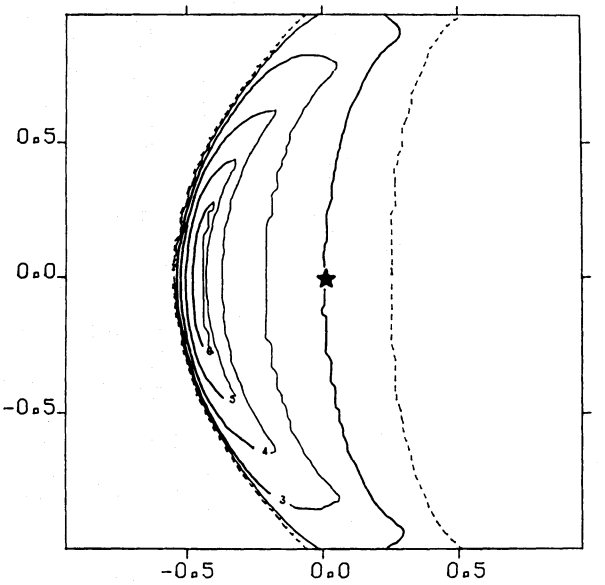

Fig. 8. Modelled infrared dust emission (arbitrary flux units). Length unit is 1 pc

very low density will develop, allowing the H II region to extend to larger radii than a homogeneous Strömgren sphere could.

Assuming steady-state conditions in a medium of constant density, we have calculated the shape of the contact discontinuity between stellar wind and shocked ISM, and of the preceding bow shock. The basic assumptions and formulae used are listed in Appendix B. In Fig. 7 the result for a star with the properties of 68 Cyg in a medium of $n_0 = 2.0\,\mathrm{cm}^{-3}$ is depicted.

Since the bow shock is optically thin in the Lyman continuum ($\tau < 5\ 10^{-3}$), it is clear that most of the H II region remains undisturbed by the stellar wind, and can thus be described as a quasi-static Strömgren sphere co-moving with the exciting star. This model is also supported by the presumed density binding in the north western part of the nebula. A part of the stellar Lc quanta can escape through the wind-depleted cone, while irregular thermal expansion (RT instabilities) of those zones may lead to a further reduction of the H II column density.

Only close to the star ($r \sim 2$–3 pc) the wind interaction becomes observationally relevant. This is valid especially in the infrared, where model calculations show that only a narrow zone ahead of the moving star produces significantly enhanced emission, while the star is located in a strongly depleted volume. The IRAS low resolution maps of some wind-driven bow shocks published by Van Buren and McCray (1988) demonstrate how prominent such structures may be if their angular scale is large enough.

Figure 8 shows the dust emission distribution for our adopted model. A comparison with the 60 μm GEISHA map allows an unambigous identification of the elongated feature, south east of the position of 68 Cyg, with the postulated bow shock.

This result enables us even to set constraints to the stellar mass loss rate: of all quantities in formula (B1), only $\dot{M}$ is largely unknown. The observed "standoff" distance star – bow shock head of about 0.5 pc does not allow $\dot{M}$ to exceed $1\ 10^{-7}\ M_\odot\ \mathrm{yr}^{-1}$ by much.

5. Conclusions

In this study we have presented observational and physical evidence that HS 240 is not a wind-driven bubble in the sense of the WEA theory. The observations are, on the other hand, completely consistent with a description of HS 240 as a classical, quasi-static Strömgren sphere ionized by and co-moving with the passing star 68 Cyg.

The classification of a stellar wind bubble based entirely on the optical, "ring like" appearance of a nebula can be very misleading. Without independent indicators such as observable expansion or a dust distribution showing a central cavity the chance of misjudging some accidental filaments for a bubble is rather high. While the gas emission rises with the density increase in the shock as n_e^2, the observable dust morphology due to its strong dependance on both density *and* temperature seems to provide a powerful diagnostic tool for bubbles and wind-driven bow shocks.

It seems to us that bubbles driven by thermal pressure from a very hot interior according to the WEA theory of "energy conservation" are not often realized in nature. While the thrown-off stellar envelopes of WR stars and PN nuclei introduce quite different boundary conditions (Icke, 1988), the number of known bubbles around single O stars is simply too low. Only one single object, NGC 7635, remains from the list of Lozinskaya (1982). There must be some physical mechanisms to prevent the formation of a hot, heat conduction-dominated interior or to cause its collapse. One such process we have studied in this paper. Whenever the blowing star moves with a velocity supersonic to the medium into which the wind is streaming an open bow shock instead of a bubble will form, with its dynamics entirely dictated by mass and momentum conservation.

As a second reason we suggest the general clumpiness of the interstellar medium, the remains of which we have observed in the still existing density fluctuations. McKee et al. (1984) have shown that due to enhanced matter protrusion through the conduction

front any hot interior will collapse soon because of a much more effective cooling if the expansion runs into a highly inhomogeneous medium. Again the future dynamics are ruled by momentum balance. If the persistence of a very hot interior is indeed the exception rather than the rule, then the time scale which let wind-driven shells around early stars stall and eventually dissipate into the embient medium becomes shorter by a factor of ~5–10.

An essential consequence of the WEA theory is the emission of soft X-rays from the bubble interior. NGC 6888 is the only bubble examined up to now in this respect with sufficient sensitivity (Kähler et al., 1987; Bochkarev, 1988), with the result that the emission is at least one order of magnitude weaker than predicted. This is just what one would expect for a recently collapsed interior, and there is no need for leaky box models, etc. When in future better X-ray observational facilities become available, it may become possible to decide finally how effective strong stellar winds can mix up the interstellar medium.

Acknowledgements. We would like to thank the directors of the Max-Planck-Institutes in Bonn and Heidelberg for granting the observation time. Support by the staff members at Calar Alto (especially U. Hopp) and Effelsberg was of great value. For the reduction of the CCD spectra we want to acknowledge the hospitality of the MPIA in Heidelberg; especially we thank Dr. J. Fried and U. Klaas for their help and admission to use some of their programs. Further, we express our thanks to Dr. P. R. Wesselius and colleagues for offering the opportunity to use the GEISHA system and for their help. Part of this work was supported by the Deutsche Forschungsgemeinschaft under grant We 741/8-1.

Appendix

A. The shell around an energy conserving bubble

The structure of the most prominent part of a bubble following the WEA theory, shell **c**, is critically dependent on the properties of the outer shock. Here we note that the compression factor as given by WEA is not correct: Their value $1+\mathcal{M}^2$ ($\mathcal{M} \equiv v_{\rm exp}/c_{II}$, isothermal Mach number) in shell **c** was derived from an erroneous form of the momentum flux conservation jump condition over the shock front. The correct factor is $\mathcal{M}^2$ (e.g. Spitzer, 1978), and then also the obviously too strong condition $\mathcal{M} \gg 1$ of WEA which would exclude most of the later bubble development becomes obsolete.

An important consequence is that the condition of trapping the ionization front and formation of a neutral shell changes. Instead of the iteration formula of WEA a simple expression for the time of capture can be written:

$$t_{\rm crit} = 3.0\, n_0^{-1}\, L_{36}^{-1}\, u_{50}^3\, 10^6\ {\rm yr}\,,$$

where $L_{36} = \frac{1}{2}\dot{M} v_\infty^2/(10^{36}\ {\rm erg\,s^{-1}})$ is the wind luminosity, and u_{50} is the excitation parameter in multiples of $50\ {\rm pc\,cm^{-2}}$.

Additionally we give the corrected formulae for the limb brightening of the bubble's emission measure:

Let $R_{\rm s} = u \cdot n_0^{-2/3}$ be the Strömgren radius of the unperturbed H II region, and R_2 the radius of the bubble (zone **b**). The distance of the ionization front to the star is then given by

$$R_I^3 = R_{\rm s}^3 - R_2^3\,(\mathcal{M}^2 - \tfrac{4}{3})\,.$$

The emission measure in the central line of sight follows to

$$\varepsilon_0 = 2 n_0^2 \left[\mathcal{M}^2 \frac{R_2}{3} + (R_I - R_2)\right],$$

while the maximum value of ε is reached with a line of sight tangentially to the contact discontinuity between **b** and **c**:

$$\varepsilon_{\rm max} = 2 n_0^2 \left[\mathcal{M}^3 R_2 \sqrt{\frac{2}{3}} + \sqrt{R_I^2 - R_2^2}\right].$$

The relative limb brightening of a bubble for the case of a just trapped *I*-front is then

$$\frac{\varepsilon_{\rm max}}{\varepsilon_0} = \mathcal{M} \cdot 3 \sqrt{\frac{2}{3}} \approx 2.45\,\mathcal{M}\,.$$

B. Shape of the bow shock

We consider an O star moving with supersonic velocity v_* into a homogeneous medium of density ϱ_0. The star loses mass at a rate of $\dot{M}$ with a terminal wind velocity v_∞. Where the wind breaks a contact discontinuity forms, lead by a shock compressing the radiatively pre-ionized interstellar medium (the second shock, moving towards the star, is in this case negligible). As Huang and Weigert (1982) have shown, such a situation may be described by a dimensionless geometry with a single scaling factor $R_1(0)$ fixing the distance of the discontinuity to the star in the direction of motion. Simply equating the ram pressures of wind and ISM yields:

$$R_1(0) = \sqrt{\frac{\dot{M} v_\infty}{4\pi \varrho_0 v_*^2}} = 1.86 \sqrt{\frac{\dot{M}_{-6} v_\infty}{n_0 v_*^2}}\ {\rm pc}\,. \qquad \text{(B1)}$$

The adopted constants for 68 Cyg are $\dot{M} = 1 \ldots 5\ 10^{-7}\, M_\odot\ {\rm yr^{-1}}$, $v_\infty = 2900\ {\rm km\,s^{-1}}$, $v_* = 42\ {\rm km\,s^{-1}}$, and $n_0 = 2\ {\rm cm^{-3}}$, leading to a value of $R_1(0) = 0.5 \ldots 1.2\ {\rm pc}$.

Since the equations by Huang and Weigert (1982) only allow a numerical solution, we simplify the analysis in so far as we neglect centrifugal forces of the offstreaming matter. The problem is then quite similar to the one described by Dyson (1975) who investigated the surface between an evaporating globule and a plane parallel wind. The shape of the discontinuity can be expressed in polar coordinates (cylinder symmetry assumed):

$$R_1(\varphi) = R_1(0)\,\frac{\varphi}{\sin\varphi}$$

To calculate the approximate structure of the leading shock we evaluate the conditions of mass and momentum conservation and assume the shock to be isothermal with a compression factor

$$\frac{\varrho_{\rm s}}{\varrho_0} = \left(\frac{v_* \sin\vartheta}{c_{II}}\right)^2 = \mathcal{M}^2(\varphi)\,,$$

where $c_{II} \simeq 11\ {\rm km\,s^{-1}}$ is the velocity of sound and

$$\vartheta = \frac{\pi}{2} - \varphi + \alpha, \quad \tan\alpha = \frac{1}{\varphi} - \tan\varphi\,.$$

The thickness of the shocked layer is

$$d = \frac{R_1(0) \cdot \varphi}{2\mathcal{M}^2(\varphi)\,\dfrac{v_\alpha}{v_*}},$$

where v_α, the velocity of the tangentially offstreaming material, is

$$\frac{v_\alpha(\varphi)}{v_*} = \frac{1}{\varphi^2} \int_0^\varphi dq\, \sqrt{q^2 - \sin^2 q}$$

with the integral to be solved numerically. In direction $\varphi = 0$ the thickness is

$$d(0) = R_1(0)\,\frac{c_{II}^2}{v_*^2}\cdot\frac{3\sqrt{3}}{2}.$$

For about $\varphi \geqq 2$ the incident velocity $v_* \sin\vartheta$ becomes subsonic and the ambient medium can react with a simple sound wave.

References

Alduseva, V.Ya., Aslanov, A.A., Kolotilov, E.A., Cherepashuck, A.M.: 1983, *Sov. Astron. Lett.* **8**, 386

Aller, L.H.: 1984, *Physics of Thermal Gaseous Nebulae*, Reidel, Dordrecht

Baars, J.W.M., Genzel, R., Pauliny-Toth, I.I.K., Witzel, A.: 1977, *Astron. Astrophys.* **61**, 99

Black, J.H., Dupree, A.K., Hartmann, L.W., Raymond, J.C.: 1980, *Astrophys. J.* **239**, 502

Bochkarev, N.G.: 1988, *Nature* **332**, 518

Bouigne, R.: 1959, *Publ. Obs. Hte. Prov.* **4**, No. 52

Castor, J., McCray, R., Weaver, R.: 1975, *Astrophys. J.* **200**, L107

Chiosi, C., Maeder, A.: 1986, *Ann. Rev. Astron. Astrophys.* **24**, 329

Chu, Y.H.: 1981, *Astrophys. J.* **249**, 195

de Loore, C.: 1978, *IAU Symp.* **83**, 313

Draine, B.T., Lee, H.M.: 1984, *Astrophys. J.* **285**, 89

Dyson, J.E.: 1975, *Astrophys. Space Sci.* **35**, 299

Dyson, J.E., Meaburn, J.: 1971, *Astron. Astrophys.* **12**, 219

Esipov, V.F., Klement'eva, A. Yu., Kovalenko, A.V., Lozinskaya, T.A., Lyutyi, V.M., Sitnik, T.G., Udal'tsov, V.A.: 1982, *Sov. Astron.* **26**, 582

Felli, M., Tofani, G., Fanti, C., Tomasi, P.: 1977, *Astron. Astrophys. Suppl.* **27**, 181

Georgelin, J.P., Georgelin, J.M.: 1970, *Astron. Astrophys.* **6**, 349

Georgelin, J.M., Lortet-Zuckermann, M.T., Monnet, G.: 1975, *Astron. Astrophys.* **42**, 273

Hänni, U., Pelt, J.: 1986, *Sov. Astron. Lett.* **12**, 228

Hase, V.F., Shajn, G.A.: 1955, *Izv. Krymsk. astrofiz. Obs.* **15**, 11

Heiles, C.: 1979, *Astrophys. J.* **229**, 533

Huang, R.Q., Weigert, A.: 1982, *Astron. Astrophys.* **116**, 348

Icke, V.: 1988, *Astron. Astrophys.* **202**, 177

Kähler, H., Ule, T., Wendker, H.J.: 1987, *Astrophys. Space Sci.* **135**, 105

Kumar, C.K., Kallmann, T.R., Thomas, R.J.: 1983, *Astrophys. J.* **272**, 219

Kurucz, R.L.: 1979, *Astrophys. J. Suppl.* **40**, 1

Lozinskaya, T.A.: 1982, *Astrophys. Space Sci.* **87**, 313

McKee, C.F., van Buren, D., Lazareff, B.: 1984, *Astrophys. J.* **278**, L115

Mezger, P.G., Henderson, A.P.: 1967, *Astrophys. J.* **147**, 471

Panagia, N., Felli, M.: 1975, *Astron. Astrophys.* **39**, 1

Pedlar, A.: 1980, *Monthly Notices Roy. Astron. Soc.* **192**, 179

Schraml, J., Mezger, P.G.: 1969, *Astrophys. J.* **156**, 269

Sharpless, S.: 1959, *Astrophys. J. Suppl.* **4**, 257

Spitzer, jr., L.: 1978, *Physical Processes in the Interstellar Matter*, Wiley, New York

Stasinska, G.: 1978, *Astron. Astrophys. Suppl.* **32**, 429

Stone, R.C.: 1979, *Astrophys. J.* **232**, 520

Van Buren, D., McCray, R.: 1988, *Astrophys. J.* **359**, L93

Weaver, R., McCray, R., Castor, J., Shapiro, P., Moore, R.: 1977, *Astrophys. J.* **218**, 377 (WEA)

Wendker, H.J.: 1971, *Astron. Astrophys.* **13**, 65

Wendker, H.J.: 1984, *Astron. Astrophys. Suppl.* **58**, 291

Wendker, H.J.: 1987, *Astron. Astrophys. Suppl.* **69**, 87

Wesselius, P.R., Bontekoe, T.R., de Jonge, A.R.W., Kester, D.J.M.: 1988: *Proc. ESO Conference No.* **28**, 85

Zeĭnalov, S.K., Musaev, F.A., Chentsov, E.L.: 1987, *Sov. Astron. Lett.* **13**, 90